International Journal of Mass Spectrometry 280 (2009) 42–49

Contents lists available at ScienceDirect

International Journal of Mass Spectrometry

journal homepage: www.elsevier.com/locate/ijms

Capture of asymmetric top dipolar molecules by ions: Rate constants for capture of H_2O, HDO, and D_2O by arbitrary ions

A.I. Maergoiz [a], E.E. Nikitin [a,b], J. Troe [a,c,*]

[a] Max-Planck-Institut für Biophysikalische Chemie, Am Fassberg 11, D-37077 Göttingen, Germany
[b] Schulich Faculty of Chemistry, Technion-Israel Institute of Technology, Haifa 3200, Israel
[c] Institut für Physikalische Chemie, Universität Göttingen, Tammannstrasse 6, D-37077 Göttingen, Germany

ARTICLE INFO

Article history:
Received 14 May 2008
Received in revised form 14 August 2008
Accepted 22 August 2008
Available online 2 September 2008

Keywords:
Ion-dipole capture
Asymmetric top
Data base for astrochemistry
Statistical adiabatic channel model

ABSTRACT

The capture of rotationally state-selected and unselected asymmetric top polar molecules by ions is investigated. Analytical expressions (for all rotational states up to $j = 2$) of capture rate constants in the perturbed-rotor second-order limit are derived for application to low temperature conditions. Approximate analytical representations over wider temperature ranges are also given for rotationally unselected molecules. The capture of H_2O, D_2O, and HDO by arbitrary ions is chosen for demonstration of the approach. Capture rate constants for the about 60 reactions of H_2O with ions listed in the UMIST 2006 data base for astrochemistry are calculated, compared with experimental data, and represented in the format $k_{cap}(T) \approx c_1 + c_2(T/300\,K)^{-1/2}$. The parameters c_1 and c_2 can be predicted in a very simple way. The approach allows one to identify capture-controlled mechanisms and/or to trace experimental artifacts. The approach applies equally well to the capture of symmetric top and linear dipole molecules by arbitrary ions.

1. Introduction

Ion–molecule reactions play an important role in astrochemistry. More than half of the about 4600 binary gas phase reactions listed in the UMIST 2006 data base for astrochemistry [1] are of this type. Under low temperature interstellar conditions, only exothermic reactions without barriers are likely to take place. They are initiated by long-range ion–molecule capture which then is followed by short-range chemical transformations into one or more reaction products or by the reverse separation of the reactants without reaction. Ion–molecule capture theory, therefore, provides upper limits of the rate constants and consequently has received considerable attention (see, e.g., refs. [2–6]).

Ion–molecule capture theory has quantum and classical aspects. At ultralow temperatures, in the μK- to mK-range, only few partial waves of the scattering process contribute and s-wave capture theory provides the quantum limit [7]. With increasing temperature, the relative translational motion becomes classical and only quantum effects from hindered-rotor type motions in anisotropic ion–molecule interaction potentials persist. We denote this range as the low temperature semi-classical limit (LTSC). The hindered-rotor type motions also become classical when kT markedly exceeds the relevant rotational constant of the neutral molecule (see, e.g., refs. [3,8]) such that vibrational quantum effects are the last to switch to classical behaviour. However, the latter need not to be considered until really high temperatures are reached. Ion–molecule capture theory according to this hierarchy may be formulated by a series of transitions between low-temperature quantum and high-temperature classical expressions. This is the concept of our SACM/CT (statistical adiabatic channel model/classical trajectory) approach to ion–molecule capture processes [9,10]. The capture of induced and permanent dipole as well as quadrupole molecules of linear and symmetric top character was treated. Within this series, the capture of asymmetric top dipoles presented particular difficulties which we reconsider in the present article. Previous studies of this problem [3,5,6] were fragmentary such that a more general formulation of the rate constants for capture of asymmetric top dipolar molecules by ions appears desirable.

The capture of the asymmetric top molecule H_2O by ions represents an important special case which, together with HDO and D_2O, in this article is chosen as an illustrative example. The UMIST 2006 data base for H_2O alone lists more than 60 of such reactions (branching pathways not counted separately). H_2O is a hydride and, therefore, has comparably large rotational constants such that quantum effects for the motion in the anisotropic ion-dipole potential persist up to temperatures in the 1–20 K range. LTSC calculations for water capture by a few ions such as N^+ and H^+

* Corresponding author at: Institut für Physikalische Chemie, Universität Göttingen, Tammannstrasse 6, D-37077 Göttingen, Germany.
E-mail address: shoff@gwdg.de (J. Troe).

1387-3806/$ – see front matter © 2008 Elsevier B.V. All rights reserved.
doi:10.1016/j.ijms.2008.08.019

have been reported before [3,5,6]. The present work generalizes these results by considering arbitrary ions, by including capture of HDO and D_2O, and by designing approximate analytical expressions for wide temperature ranges. We try to keep the recommended expressions as simple as possible, but we have to go beyond the format $k_{cap}(T) = c(T/300\,K)^n$ used so far in the UMIST data base [1]. A comparison of the calculated capture rate constants with values included in the data base permits to identify either experimental errors or the effects of reverse dissociations of the collision complexes without that reaction has taken place. We do not restrict our work to thermal capture rate constants of rotationally unselected molecules but we also consider rate constants for rotationally state-selected molecules.

2. Representation of thermal capture rate constants

We intend to provide expressions of the capture rate constant $k_{cap}(T)$ which interpolate between the low-temperature semi-classical limit, $k_{cap,0}$, and the high-temperature classical limit, $k_{cap,\infty}$. Before doing this, a few remarks are important. (i) We here do not consider the quantum limit of $k_{cap}(T)$ at $T = 0$ K [7] but only the semi-classical low-temperature limit $k_{cap,0}$, where the translation is classical but the hindered rotor-type motion is in its quantum limit. Throughout this article by "$T \to 0$" we refer to this temperature range. (ii) It is common knowledge that ion-induced dipole capture, showing no such hindrance of the rotations, is characterized by the Langevin rate constant

$$k_L = 2\pi q \left(\frac{\alpha}{\mu}\right)^{1/2} \tag{2.1}$$

independent of the temperature (μ = reduced mass of the collision pair, α = isotropic polarizability of the neutral molecule). In this case, $k_{cap,0}$ and $k_{cap,\infty}$ are identical and equal to k_L (we note that Eq. (2.1) does not represent the true quantum limit, which is given by $2k_L$ and which is only approached in the μK- to mK-range [7], but only the semi-classical low-temperature limit $k_{cap,0}$). (iii) At high temperatures, the effective bottle-neck of the reaction moves from the long-range electrostatic to the short-range valence potential. We neglect the latter and only analyze capture in the long-range potential. (iv) We consider capture in a single electronic state and assume that complications by the presence of multiple electronic states are included in the dynamics of the collision complex treated separately from the capture calculations.

General expressions for $k_{cap}(T)$ were obtained from the reduced representation of capture rate-constants from ref. [8] for the capture of ions by linear dipoles which interpolates between $k_{cap,0}$ and $k_{cap,\infty}$. Employing a LTSC SACM treatment, it was shown that $k_{cap}(T)$ can very well be expressed in the form

$$\frac{k_{cap}(T)/k_L - 1}{k_{cap,0}/k_L - 1} \approx 1 - 0.065y^{1.3} - 0.069y^{3.8} \tag{2.2}$$

for $y < 1$, and

$$\frac{k_{cap}(T)/k_L - 1}{k_{cap,\infty}/k_L - 1} \approx 1 - 0.134y^{-4.2} \tag{2.3}$$

for $y > 1$, where

$$y = \frac{k_{cap,0}/k_L - 1}{k_{cap,\infty}/k_L - 1} \tag{2.4}$$

represents a reduced variable related to the temperature. When $k_{cap,\infty}$ decreases with increasing temperature and $k_{cap,0}$ is temperature independent, y increases with increasing temperature. Eqs. (2.2)–(2.4) in ref. [8] were shown to reproduce individual quantum SACM calculations for ion-linear dipole capture within about 1%.

Applying Eqs. (2.1)–(2.4) to specific reactions requires the knowledge of $k_{cap,0}$ and $k_{cap,\infty}$. $k_{cap,0}$ follows from the perturbation limit of SACM (or ACCSA, perturbed rotor or similar other approaches [4]) which corresponds to the earlier elaborated expressions of weak-field Stark spectroscopy (see ref. [11]). For asymmetric top dipoles, e.g., the results for individual rotational states were tabulated numerically by Golden and Wilson [12] and they were found to be in perfect agreement with the analytical results of our work, see Section 3. For the capture of H_2O, this leads to thermal rate constants [6,8]

$$\frac{k_{cap,0}}{k_L} = \left[1 + \frac{2\mu_{D,b}^2}{3\alpha(A+C)}\right]^{1/2} \tag{2.5a}$$

where $A > B > C$ are the rotational constants of the asymmetric top (in energy units) and μ_D is the dipole moment which, for H_2O, has only the component $\mu_{D,b}$ along the b-axis (we adhere to the nomenclature from ref. [13] where the a, b, and c axes correspond to the rotational constants A, B, and C). For HDO, besides $\mu_{D,b}$ there is also a component $\mu_{D,a}$ along the a-axis and $k_{cap,0}$ then is given by [8,14]

$$\frac{k_{cap,0}}{k_L} = \left[1 + \frac{2\mu_{D,b}^2}{3\alpha(A+C)} + \frac{2\mu_{D,a}^2}{3\alpha(B+C)}\right]^{1/2} \tag{2.5b}$$

The high-temperature limit $k_{cap,\infty}$ so far has been studied less systematically. For the capture of linear dipoles, approximate analytical adiabatic channel calculations, which cover the full transition from weak to strong field Stark effect [15], gave the same results as classical trajectory calculations in the adiabatic dynamical limit [8,9]. The latter were analytically represented also by Su and Chesnavich (for the original work, see ref. [16]; minor improvements were given later [8,17]). The classical trajectory calculations from ref. [9], however, provided more general analytically fitted expressions which apply to the full range from adiabatic to nonadiabatic dynamical behaviour. Treatments for asymmetric tops in the adiabatic limit exist only for very few specific examples. There is, therefore, some need to do systematic CT calculations from the adiabatic to the nonadiabatic limit. As long as these are not available, we recommend the following procedure. It was shown in ref. [8], for capture of H_2O and NH_3 by N^+, that differences between classical capture rate constants for asymmetric and symmetric tops and linear rotors are only small. We, therefore, suggest to represent $k_{cap,\infty}$ by the same results as obtained from CT calculations for linear rotors, i.e., by Eqs. (2.1)–(2.4), and to correct for deviations from these results by the use of an effective dipole moment $\mu_{D,eff}$ in the expression for $k_{cap,\infty}$. The effective dipole moment should be calibrated by selected accurate SACM or CT calculations and then be used quite generally. This will be the strategy followed in the present work.

The procedure outlined above can be elaborated for capture of H_2O by ions, using for calibration our numerical calculations described in Section 3 which go beyond the results for $H_2O + N^+$ from Dubernet and McCarroll of ref. [5]. Using the molecular parameters given in Appendix A.1, Eq. (2.5) for capture of H_2O by arbitrary ions leads to

$$\frac{k_{cap,0}}{k_L} = 14.77 \tag{2.6}$$

When slightly different molecular parameters are chosen, e.g., the parameters selected in ref. [5], Eq. (2.5a) allows one to accommodate for that. $k_{cap,\infty}$, on the other hand, will be represented by the simple Su–Chesnavich expression

$$\frac{k_{cap,\infty}}{k_L} = 0.4767x + 0.6200 \quad \text{for } x \geq 2 \tag{2.7a}$$

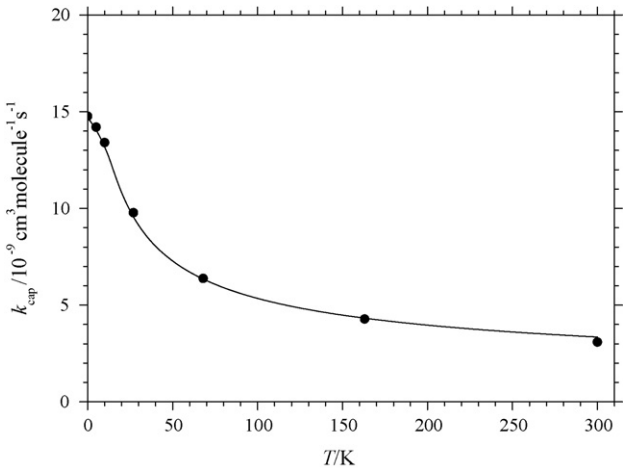

Fig. 1. Rate constants $k_{cap}(T)$ for $H_2O + N^+$ (full line: representation by Eqs. (2.1)–(2.4), (2.5a) and (2.7a) with $\mu_{D,eff}/\mu_D = 1.07$, see text: (●) experimental points for $T \geq 27$ K from refs. [18–20] and calculations for $T \leq 10$ K from refs. [3] and [5]).

$$\frac{k_{cap,\infty}}{k_L} = \frac{(x + 0.5090)^2}{10.526} + 0.9754 \quad \text{for } x \leq 2 \tag{2.7b}$$

with $x = \mu_{D,eff}/(2\alpha kT)^{1/2}$. Comparing Eqs. (2.1)–(2.7) with the numerical data for $H_2O + N^+$ from Section 3 gives $\mu_{D,eff} = 1.07\,\mu_{D,b}$, see below. The difference between the true $\mu_{D,b}$ and the fitted $\mu_{D,eff}$ as suggested above indeed is small. Having adjusted $\mu_{D,eff}$ in this way, the complete temperature dependence of k_{cap} for $H_2O + N^+$ can be represented such as done in Fig. 1 (with $k_L = 1.00 \times 10^{-9}$ cm^3 molecule^{-1} s^{-1}). One observes that the experimental data between 27 and 300 K from refs. [18–20] nearly coincide with our representation which confirms the earlier conclusions about a complete capture control of the reaction.

Inspecting Fig. 1, one may draw a number of conclusions. (i) The transition to the low temperature quantum range takes place only at temperatures below 20 K. (ii) The temperature range 20–300 K corresponds to $x \geq 2$ such that only the Su–Chesnavich expression (2.7a) is of relevance. An alternative might be the simplified expression [8]

$$k_{cap,\infty} \approx k_L + f_{rigid} k_{ld} \tag{2.8}$$

with a "rigidity factor" $f_{rigid} = 1/2$ and a "locked dipole capture rate constant" k_{ld} given by $k_{ld} = 2\pi q \mu_{D,eff} \sqrt{2/\pi\mu kT}$. One then would have

$$\frac{k_{cap,\infty}}{k_L} \approx 1 + \left(\frac{\mu_{D,eff}^2}{2\pi\alpha kT} \right)^{1/2} \tag{2.9}$$

over the full range of the parameter x. However, Eq. (2.7a) performs better for the low temperature range $x \geq 2$ of relevance here. Fig. 2 provides a comparison of Eq. (2.9) with Eq. (2.7a) and the complete numerical results from Eqs. (2.1)–(2.7a). The first improvement for empirical representations of $k_{cap}(T)$ beyond a simple power law $k_{cap}(T) \approx c(T/300\,\text{K})^{-1/2}$, therefore, would be the use of $k_{cap}(T) \approx c_1 + c_2(T/300\,\text{K})^{-1/2}$. The divergence of this expression for $T \to 0$ is an artifact due to the neglect of quantum effects in the hindered rotor motion. This could be accounted for by putting

$$k_{cap}(T) = \min \left\{ k_{cap,0}, c_1 + c_2 \left(\frac{T}{300\,\text{K}} \right)^{-1/2} \right\} \tag{2.10}$$

with $k_{cap,0}$ from Eq. (2.5a). On the other hand, the high-temperature limit c_1 finally will also become unphysical because, under real high temperature conditions, the contributions of a short-range valence potential will replace those of the ion-induced dipole potential. (iii) Changing the ion will only influence the reduced mass μ of the collision pair. This can be accounted for by a simple scaling of the rate constant according to the respective k_L. We shall exploit this behaviour in Section 4. Comparing Eq. (2.10) with Eqs. (2.6) and (2.7a) defines the values of the parameters $k_{cap,0}$, c_1, and c_2 to be used for practical applications, see Section 4.

3. Representation of rotationally state-selected rate constants

Before we compare the described representation of thermal capture rate constants with the values of the UMIST data base, we consider rotationally state-selected rate constants for capture of H_2O, D_2O, and HDO by ions. We divide our discussion into two parts: first we derive accurate analytical expressions of the limiting low-temperature capture rate constants for rotational quantum numbers (j,τ) of the asymmetric top up to $j = 2$. After that we provide thermal rate constants for unselected molecules employing extended SACM calculations with contributions from large ranges of j (up to $j = 10$), which have also been used for the calibration of $\mu_{D,eff}$ in Section 2.

In order to derive low-temperature limiting rate constants, we construct perturbed-rotor adiabatic channel potential curves $V^{PR}_{j,\tau,m}(R)$ which converge to the energy levels $E_{j,\tau}$ of the free asymmetric top. The $V^{PR}_{j,\tau,m}(R)$ are composed of second-order charge-permanent dipole (cd) terms $V^{cd,2}_{j,\tau,m}(R)$, first-order charge-permanent quadrupole (cq) terms $V^{cq,1}_{j,\tau,m}(R)$, and charge-induced dipole (cid) terms $V^{cid}_{j,\tau,m}(R)$, i.e.,

$$V^{PR}_{j,\tau,m}(R) = V^{cd,2}_{j,\tau,m}(R) + V^{cq,1}_{j,\tau,m}(R) + V^{cid}_{j,\tau,m}(R) \tag{3.1}$$

where R denotes the center-of-mass distance between the ion and neutral species. In the following we concentrate on the contribution from the first term for the case of a planar rotor which has only two independent rotational constants, i.e., $1/C = 1/A + 1/B$. Calculating the charge-dipole interaction energy in second order for states with $j = 0$, 1, and 2, we resort on analytical expressions for the energy levels $E_{j,\tau}$ and the eigenfunctions $|j,\tau,m>$ for $j = 0$, 1, 2, and 3. The latter are used for calculating the matrix elements $<j,\tau,m|\mu_{Dg}|j',\tau',m'>$ of the component μ_{Dg} of the dipole moment along the axes g of the body-fixed frame of the principal moments of inertia. Again, for the planar rotor, the dipole moment has only the non-vanishing components $\mu_{D,a}$ and $\mu_{D,b}$, see above.

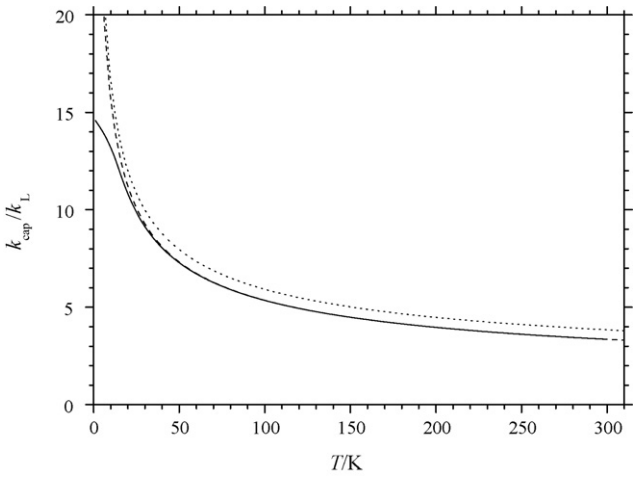

Fig. 2. Comparison of $k_{cap}(T)/k_L$ for capture of H_2O by ions from approximate representations (full line: Eqs. (2.2)–(2.4), (2.5a) and (2.7a), dashed line: Eq. (2.7a), dotted line: Eq. (2.9), with $\mu_{D,eff}/\mu_D = 1.07$, see text).

Table 1
Second-order coefficients $A_{gj\tau}$ and $B_{gj\tau}$ in Eq. (3.5) for rotational states (j,τ)

	j,τ								
	0,0	1,−1	1,0	1,1	2,−2	2,−1	2,0	2,1	2,2
H_2O									
$A_{bj\tau}\times10^2$	−100/6	−6.59	−8.13	−4.03	0.746	0.806	−2.38	0.372	−1.08
$B_{bj\tau}\times10^2$	–	−24.3	−14.5	26.9	−6.08	−1.96	3.52	0.359	1.68
D_2O									
$A_{bj\tau}\times10^2$	−100/6	−6.71	7.58	−3.99	1.11	0.609	−2.38	0.074	−4.72
$B_{bj\tau}\times10^2$	–	−22.9	−14.4	25.6	−6.46	−1.91	4.15	0.348	1.72
HDO									
$A_{bj\tau}\times10^2$	−100/6	−6.93	5.96	−3.91	2.43	0.041	−2.38	−1.81	3.36
$B_{bj\tau}\times10^2$	–	−20.7	−14.0	23.4	−7.07	−1.80	4.82	0.488	0.385
$A_{aj\tau}\times10^2$	−100/6	9.95	−5.45	−4.62	2.33	1.28	1.09	−2.38	−2.28
$B_{aj\tau}\times10^2$	–	−15.0	−74.2	76.7	−1.20	−3.70	2.04	−261.9	262.5

The second-order cd-term is quadratic in the quantum number m and can be written as

$$V^{\mathrm{cd},2}_{j,\tau,m}(R)=\sum_g \frac{\mu^2_{\mathrm{Dg}}q^2}{B_{\mathrm{eff},g}R^4}[A_{gj\tau}(\kappa,\eta)+m^2B_{gj\tau}(\kappa,\eta)] \tag{3.2}$$

where g = a, b, and c and $\kappa=(2B-A-C)/(A-C)$ and $\eta=(A-C)/(A+C)$. $B_{\mathrm{eff},g}$ stands for the rotational constants $B_{\mathrm{eff},b}=(A+C)/2$ and $B_{\mathrm{eff},a}=(B+C)/2$. Analytical results for the quantities $A_{gj\tau}$ and $B_{gj\tau}$ for $j\le2$ are given in Appendix A.2. For a planar top, κ and η can also be expressed by a single parameter $\gamma=C/A$ such that $A_{gj\tau}$ and $B_{gj\tau}$ with $\kappa=(\gamma^2+2\gamma-1)/(1-\gamma)^2$ and $\eta=(1-\gamma)/(1+\gamma)$ become functions $\tilde{A}_{gj\tau}(\gamma)$ and $\tilde{B}_{gj\tau}(\gamma)$, see Appendix A.2.

Neglecting the generally small charge-quadrupole contribution and assuming that the charge-induced dipole term is isotropic, the adiabatic channel potential curves take the form

$$V^{\mathrm{eff}}_{j,\tau,m}(R)=\frac{-q^2\alpha^{\mathrm{eff}}_{j,\tau,m}}{2R^4} \tag{3.3}$$

with an "effective polarizability" $\alpha^{\mathrm{eff}}_{j,\tau,m}$ given by

$$\alpha^{\mathrm{eff}}_{j,\tau,m}=\alpha-\sum_g\frac{2\mu^2_{\mathrm{Dg}}[\tilde{A}_{gj\tau}(\gamma)+m^2\tilde{B}_{gj\tau}(\gamma)]}{B_{\mathrm{eff},g}} \tag{3.4}$$

Adding centrifugal energy $l(l+1)\hbar^2/2\,\mu R^2$ and determining the adiabatic channel maxima $E_0(j,m,\tau,l)$ leads to "activated complex partition functions" [3,8] and from that to thermal capture rate constant in the perturbed-rotor limit. For $T\to0$, one obtains the

Table 2
Capture rate constants $k_{\mathrm{cap}}/10^{-9}$ cm^3 molecule^{-1} s^{-1} from numerical adiabatic channel calculations (the upper lines for H_2O+N^+ are from the present work, the lower lines from ref. [5], see text)

Reaction	T (K)	Therm	j,τ								
			0,0	1,−1	1,0	1,1	2,−2	2,−1	2,0	2,1	2,2
H_2O+N^+	→0	14.77	14.77	16.49	6.13	2.44	10.38	5.46	1.13	0.	0.78
	5	14.2	14.2	15.5	6.2	2.46	9.6	5.2	2.27	2.56	1.59
		14.8	14.8	15.6	6.7	2.6	10.2	5.5	2.3	4.3	2.6
	10	13.4	13.5	14.04	6.44	2.77	9.26	5.36	3.0	3.52	2.19
		13.9	14.1	14.4	6.9	2.9	9.8	5.6	3.0	4.9	3.1
	27	9.78	11.75	11.62	6.64	3.77	8.35	5.48	4.0	4.53	3.12
		10.1	12.3	12.1	7.0	3.9	8.8	5.7	3.9	5.4	3.7
	68	6.38	9.47	9.17	6.31	4.54	7.13	5.31	4.47	4.80	3.65
		6.6	9.7	9.4	6.6	4.7	7.4	5.5	4.4	5.3	4.0
	163	4.28	7.27	7.03	5.52	4.57	5.85	4.82	4.36	4.50	3.73
		3.2	5.2	5.4	5.0	4.2	4.8	4.3	4.1	4.2	3.6
	300	3.09	5.92	5.75	4.82	4.25	4.99	4.33	4.03	4.09	3.57
		2.3	3.0	3.3	3.4	2.8	3.1	2.9	2.6	3.0	2.6
D_2O+N^+	→0	19.53	19.53	21.48	8.34	3.20	13.95	7.30	1.49	0.	5.42
	5	17.93	18.01	18.79	8.84	3.61	12.34	7.01	3.37	2.61	4.94
	10	15.13	16.57	16.62	9.08	4.49	11.53	7.19	4.43	3.46	5.13
	27	9.67	13.54	13.16	8.79	5.83	9.90	7.15	5.58	4.46	5.31
	68	6.30	10.33	9.98	7.72	6.14	8.10	6.58	5.76	4.82	5.20
	163	4.10	7.63	7.41	6.29	5.53	6.40	5.62	5.21	4.55	4.73
	300	2.80	6.10	5.95	5.29	4.84	5.33	4.85	4.59	4.13	4.24
HOD + N^+	→0	17.20	17.20	15.85	13.75	2.85	10.75	7.29	1.08	39.97	0.
	5	15.87	15.86	16.21	9.45	2.93	9.42	5.35	1.63	1.69	0.04
	10	14.17	14.63	14.49	9.13	3.63	8.96	5.59	2.55	2.28	0.28
	27	9.47	12.08	11.80	8.47	5.17	8.14	5.88	4.16	3.30	1.35
	68	6.17	9.36	9.10	7.30	5.61	7.07	5.69	4.88	3.96	2.62
	163	4.10	7.02	6.84	5.91	5.08	5.80	5.01	4.65	3.98	3.24
	300	2.88	5.67	5.54	4.97	4.48	4.91	4.39	4.19	3.73	3.25

m-degeneracy averaged values

$$k_{j,\tau}^{\mathrm{PR}} = \frac{k_{\mathrm{L}}}{2j+1}\sum_{m=-j}^{j}\left\{1-\sum_{g}\frac{2\mu_{\mathrm{Dg}}^2[\tilde{A}_{gj\tau}(\gamma)+m^2\tilde{B}_{gj\tau}(\gamma)]}{\alpha B_{\mathrm{eff},g}}\right\}^{1/2} \quad (3.5)$$

which, for $j=\tau=m=0$ and $A_{b\,0\,0}=-1/6$ include Eq. (2.5a) for H_2O and D_2O (and Eq. (2.5b) for HDO).

We proceed to a numerical evaluation of the state-selected capture rate constants $k_{j,\tau}^{\mathrm{PR}}(T\to 0)$ from Eq. (3.5). We note that the numerical results tabulated in ref. [12] perfectly agree with the analytical expressions for the $A_{gj\tau}$ and $B_{gj\tau}$ derived here and summarized in Appendix A.2. Table 1 shows the corresponding numerical values for H_2O, D_2O, and HDO up to $j=2$.

Extending the calculations beyond the low temperature limit characterized by second-order perturbed-rotor behaviour can either be done by classical trajectory calculations, such as described for linear rotors in refs. [9,16], by interpolation between weak-field and strong-field Stark effect expressions, such as described for symmetric tops in refs. [3,15], or by numerical adiabatic channel eigenvalue calculations through individual matrix diagonalizations (see, e.g., refs. [5,6]). In the present work we have chosen the latter approach including channels up to $j=10$. Table 2 presents our results. Thermal rate constants are given for capture of H_2O, D_2O, and HDO by N^+ such that a comparison with the previous data from ref. [5] can be made. Rate constants for rotationally selected (up to $j=2$) and rotationally unselected molecules are given. For $N^+ + H_2O$, the table also includes the values from ref. [5]. The temperatures $T\to 0$, 5, 10, 27, 68, 163, and 300 K are chosen like in the measurements of ref. [18] and in the calculations of ref. [5] (except $T\to 0$ K). A number of observations are made such as described in the following.

(i) Our results for k_{cap} of unselected H_2O agree well with the data from ref. [5] up to 68 K. The small differences are at least in part due to the slight differences in the used molecular parameters. However, at 163 and even more at 300 K, the data from ref. [5] fall markedly below the present results. This is probably due to the use of smaller numbers of channels in ref. [5]. The symmetric top calculations for $N^+ + H_2O$ from ref. [21] had a similar problem, leading to markedly too small values of $k_{\mathrm{cap}}(T)$ at 300 K. One should also note that we have accounted for proper nuclear spin-statistical weights in our work.

(ii) The values for $k_{\mathrm{cap}}(T)$ of rotationally state-selected H_2O up to $j=1$ from ref. [5] are also in good agreement with the present results up to 68 K, but at higher temperatures they fall below our results for the same reasons as indicated in (i).

(iii) For $j=2$, there are larger disagreements between ref. [5] and the present results even at low temperatures which must be numerical artifacts.

(iv) The rotationally state-selected values of $k_{\mathrm{cap}}(T)$ have quite varying temperature dependences. For some channels, $k_{\mathrm{cap}}(T)$ increases with increasing temperatures before it decreases; for other channels, it only decreases. The same phenomenon was documented for ion-linear dipole capture in ref. [3] and can be attributed to the partly repulsive, partly attractive character of the adiabatic channel potential curves for the channels (j,τ,m) included in the averaging over m.

(v) One observes that $k_{\mathrm{cap}}(T)$ approaches zero for $T\to 0$ K, when $(j,\tau)=(2,1)$ for H_2O and D_2O, but does not do that for HDO, where zero is approached for $(j,\tau)=(2,2)$ in contrast to H_2O and D_2O. This effect is due to differences in the complicated pattern of dipole coupling between different rotational levels. The behaviour then changes dramatically for $T>0$ because of early pseudocrossings of channels.

(vi) One finally notes that the perturbed-rotor results characterizing $k_{\mathrm{cap}}(T)$ at $T\to 0$ K only for j up to $j=1$ provide useful estimates for $k_{\mathrm{cap}}(T)$ and they do it only up to 10 K. At larger j and higher temperatures higher-order terms and repulsive potentials result in increasingly strong deviations from $k_{\mathrm{cap}}(T)$ at $T\to 0$ K.

Table 3
Comparison of calculated and fitted capture rate constants for $H_2O + N^+$ ($k_{\mathrm{cap}}(T)/k_{\mathrm{L}}$ (calc) from numerical adiabatic channel results of Section 3, $k_{\mathrm{cap}}(T)/k_{\mathrm{L}}$ (fit) from Eqs. (2.1)–(2.7), see text

T (K)	$k_{\mathrm{cap}}(T)/k_{\mathrm{L}}$ (calc)	$k_{\mathrm{cap}}(T)/k_{\mathrm{L}}$ (fit)
→0	14.77	14.77
1	–	14.58
5	14.2	14.05
10	13.2	13.18
20	–	10.82
27	9.78	9.58
50	–	7.28
68	6.38	6.35
80	–	5.90
120	–	4.94
163	4.28	4.33
200	–	3.97
250	–	3.61
300	3.09	3.35

In Table 2 we compare the analytical approximation from Eqs. (2.1)–(2.5) for $k_{\mathrm{cap}}(T)/k_{\mathrm{L}}$ with the present results and results from ref. [5] for selected temperatures. One should note that the fit parameter $\mu_{\mathrm{D,eff}}/\mu_{\mathrm{D},b}=1.07$ of the approximation (also used in Fig. 1) was based on the calculated points up to 68 K. Inspection of the numerical results from Table 3 suggests that even the present calculations up to $j=10$ may slightly underestimate the true values for 300 K. This emphasizes even more the necessity to resort on the analytical approximation of Eqs. (2.1)–(2.5).

Table 2 includes data for capture of H_2O, D_2O, and HDO by N^+. These results again are well reproduced by Eqs. (2.1)–(2.5). However, instead of $\mu_{\mathrm{D,eff}}/\mu_{\mathrm{D},b}=1.07$ for H_2O, we obtain $\mu_{\mathrm{D,eff}}/\mu_{\mathrm{D},b}=1.06$ for D_2O and $\mu_{\mathrm{D,eff}}/\mu_{\mathrm{D}}=1.04$ for HDO. (In the latter case, with the two components $\mu_{\mathrm{D},b}=0.675$ D and $\mu_{\mathrm{D},b}=1.730$ D, we have used $\mu_{\mathrm{D}}=(\mu_{\mathrm{D},a}^2+\mu_{\mathrm{D},b}^2)^{1/2}=1.857$ D.) The differences between the fitted ratios $\mu_{\mathrm{D,eff}}/\mu_{\mathrm{D}}$ appear to be within the uncertainties of the fitting procedure and the numerical calculations. We note that the agreement between the selected numerical points and the representation by Eqs. (2.1)–(2.5) for D_2O and HDO is similarly satisfactory as for H_2O.

Fig. 3 illustrates $k_{\mathrm{cap}}(T)/k_{\mathrm{L}}$ for rotationally state-selected H_2O. All channels up to $j=2$ are shown. One may also try to represent these results in analytical form analogous to Eqs. (2.1)–(2.5). A comparison with the results for ion-linear dipole capture from ref.

Table 4
Comparison of experimental and calculated rate constants (in 10^{-9} cm^3 molecule^{-1} s^{-1}; a: experimental data from ref. [18], b: modelling by Eqs. (2.1)–(2.4), (2.5a) and (2.7a), c: numerical adiabatic channel calculations from this work)

	T (K)				Note
	27	68	163	300	
$He^+ + H_2O$	4.3	1.8	–	0.45	a
	15	9.9	6.7	5.2	b
$C^+ + H_2O$	12	5.2	–	2.5	a
	10	6.7	4.5	3.5	b
$N^+ + H_2O$	9.9	6.0	3.8	2.8	a
	9.6	6.4	4.3	3.4	b
	9.8	6.4	4.3	3.1	c

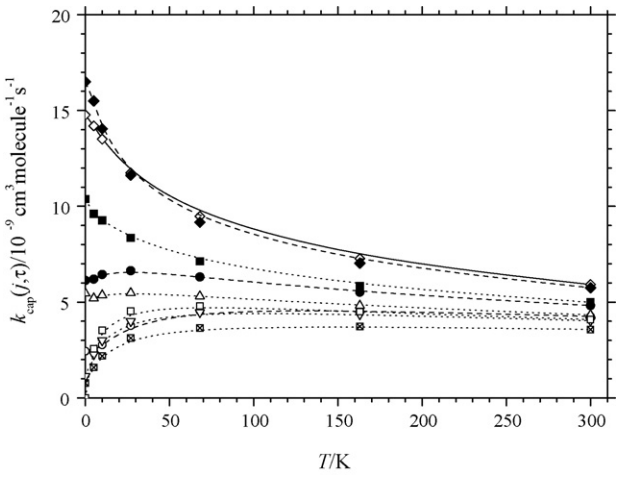

Fig. 3. Rotationally state-selected rate constants $k_{cap}(T)$ (in 10^{-9} cm^3 molecule^{-1} s^{-1}) for capture of H_2O by N^+ (symbols: adiabatic channel calculations from the present work; the lines are spline fits to guide the eyes; j,τ = 0,0 (◇); 1,−1 (◆); 1,0 (●); 1,1 (○); 2,−2 (■); 2,−1 (△); 2,0 (▽); 2,1 (□); 2,2 (⊠)).

[3] (see Fig. 10 of ref. [3]) shows that the transition from the low temperature limit of $k_{cap}(T)$ to $k_{cap,\infty}$ extends up to much higher temperatures than for unselected molecules. Furthermore, $k_{cap,0}$ in general cannot be taken from a perturbed-rotor treatment anymore. Instead, one would have to extract $k_{cap,0}$ from the numerical results for low temperatures. We do not further proceed towards an analytical representation. The lines in Fig. 3 instead are only drawn to guide the eye.

4. Comparison of experimental data with calculated capture rates

While there are no experimental results for the reactions of rotationally state-selected H_2O with ions, the UMIST data base includes a large number of data for thermal rate constants. However, only few of the reported studies extend down to temperatures where one could hope to see a transition from the classical expression (2.7) to the perturbed-rotor LTSC results of Eq. (2.5). Inspecting the exceptional experiments by Marquette et al. [20], which go down to 27 K, Fig. 1 shows that even at 27 K a substantial deviation from the classical expression (2.7) is not yet observable. The experiments for the reaction $C^+ + H_2O$ again gave nearly the same rate constants as Eq. (2.7). On the other hand, the excellent agreement between the experiments over the range 27–300 K and Eq. (2.7) indicates that the reactions $N^+ + H_2O$ and $C^+ + H_2O$ indeed are capture-controlled. Experimental results for $He^+ + H_2O$ were markedly below the predictions from Eq. (2.7), see Table 4. Either the mechanism of the latter reaction is not governed by capture-control or there have been experimental problems.

In Table 5 we systematically compare experimental data for 300 K, such as compiled in the UMIST 2006 data base [1], with the capture calculations of the present work using Eq. (2.7a) with the appropriate $\mu_{D,eff} = 1.07\mu_D$ such as specified in Section 3. According to our treatment, the capture rates are only functions of $k_{cap,\infty}/k_L$, such that the various systems should differ only by the reduced masses μ in their respective values of k_L. Differences between experiment and theory in Table 5, therefore, should either indicate experimental errors, particularly when the experimental value k_{exp} exceeds $k_{cap}(T)$, or point towards back-dissociation of the ion–water complex such that $k_{exp} < k_{cap}(T)$. One notices that about one half of the 60 reactions included in Table 5 within experimental uncertainties at T = 300 K have values of k/k_L in the range 2–4.6. The average of k/k_L within this group is equal to 3.07 which is in very good agreement with our calculated value of 3.09 for 300 K given in Table 2. We conclude that all these reactions (labelled by + in Table 5) are capture-controlled. The deviations of their measure k/k_L at 300 K from the value 3.09 most likely then corresponds to experimental uncertainty. Their rate constants furthermore should

Table 5
Rate constants for reactions of H_2O with ions at 300 K (reactions from the UMIST 2006 data base [1]. k = experimental values in 10^{-9} cm^3 molecule^{-1} s^{-1} as compiled in ref. [1]; k_L = Langevin capture rate constants in 10^{-9} cm^3 molecule^{-1} s^{-1}; cap:+ stands for k/k_L in the range 2.0–4.6, presuming capture control; cap: − stands for $k/k_L < 2.0$; c_1 and c_2 in 10^{-9} cm^3 molecule^{-1} s^{-1} are the parameters of Eq. (4.1), see text)

Ion	k	k_L	k/k_L	cap	c_1	c_2
C^+	2.70	1.050	2.57	+	0.65	2.87
C^-	0.50	1.050	0.48	−	0.65	2.87
CH^+	4.06	1.026	3.96	+	0.64	2.80
CH_2^+	1.20	1.004	1.20	−	0.62	2.74
CH_3^+	0.002	0.985	0.00	−	0.61	2.69
CH_4^+	2.60	0.968	2.69	+	0.60	2.65
CH_5^+	3.70	0.953	3.88	+	0.59	2.60
H^+	6.90	2.887	2.39	+	1.79	7.89
H^-	3.8	2.887	1.32	−	1.79	7.89
H_2^+	7.3	2.094	3.49	+	1.30	5.72
C_2^+	0.88	0.879	1.00	−	0.54	2.40
C_2H^+	0.87	0.871	1.00	−	0.54	2.38
$C_2H_2^+$	0.22	0.864	0.25	−	0.54	2.36
$C_2H_3^+$	1.11	0.858	1.29	−	0.53	2.34
$C_2H_5^+$	1.40	0.846	0.92	−	0.52	2.31
C_2N^+	0.315	0.807	0.39	−	0.50	2.21
$C_2N_2^+$	2.4	0.771	3.11	+	0.48	2.11
C_3H^+	0.45	0.810	0.56	−	0.50	2.21
C_3O^+	0.5	0.771	0.65	−	0.48	2.11
C_4N^+	1.5	0.755	1.99	−	0.47	2.06
$C_2H_6^+$	2.95	0.840	3.51	+	0.52	2.30
CN^+	2.88	0.864	3.33	+	0.54	2.36
CNC^+	1.63	0.807	2.02	+	0.50	2.21
CO^+	2.604	0.852	3.06	+	0.53	2.33
CO_2^+	2.796	0.789	3.54	+	0.49	2.16
H_2Cl^+	2.00	0.809	2.47	+	0.50	2.21
H_2CO^+	2.60	0.840	3.09	+	0.52	2.30
H_2S^+	0.81	0.821	0.99	−	0.57	2.24
H_3CO^+	0.23	0.835	0.28	−	0.52	2.28
HCN^+	3.60	0.858	4.20	+	0.53	2.34
HCO^+	2.50	0.846	2.96	+	0.52	2.31
HCO_2^+	2.30	0.786	2.93	+	0.49	2.15
$HCOOH_2^+$	0.021	0.781	0.03	−	0.48	2.13
HN_2^+	2.60	0.846	3.07	+	0.52	2.31
HNO^+	2.30	0.835	2.75	+	0.52	2.28
$HNSi^+$	2.00	0.791	2.53	+	0.49	2.16
$HOCS^+$	3.40	0.756	4.50	+	0.47	2.07
HPO^+	0.34	0.779	0.44	−	0.48	2.13
HS^+	0.78	0.826	0.94	−	0.51	2.26
$HSiS^+$	1.10	0.756	1.46	−	0.47	2.07
HSO_2^+	2.13	0.751	2.84	+	0.47	2.05
N_2^+	2.80	0.852	3.29	+	0.53	2.33
N_2O^+	2.289	0.789	2.90	+	0.49	2.15
$NCCNH^+$	0.51	0.769	0.66	−	0.48	2.10
O_2H^+	0.82	0.826	0.99	−	0.51	2.26
P^+	0.55	0.836	0.66	−	0.52	2.28
PH^+	1.20	0.831	1.44	−	0.52	2.27
PH_2^+	0.49	0.826	0.59	−	0.51	2.26
Si^+	0.23	0.851	0.27	−	0.53	2.33
$SiCH_3^+$	2.00	0.791	2.53	+	0.49	2.16
SiH^+	0.80	0.845	0.95	−	0.52	2.31
SiH_4^+	2.00	0.830	2.41	+	0.51	2.27
SiH_5^+	2.00	0.826	2.42	+	0.51	2.26
H_3^+	5.90	1.753	3.37	+	1.09	4.79
He^+	0.5505	1.558	0.35	−	0.97	4.26
N^+	2.80	1.005	2.79	+	0.62	2.75
NH^+	3.325	0.985	3.38	+	0.61	2.69
NH_2^+	3.005	0.968	3.10	+	0.60	2.65
NH_3^+	0.110	0.927	0.12	−	0.57	2.53
OH^+	2.89	0.953	3.03	+	0.59	2.60

have a temperature dependence given by Eqs. (2.1)–(2.7a) or, simplified, by Eqs. (2.8)–(2.10). Following Eq. (2.7a), Table 5 includes the parameters $c_1 = 0.62k_L$ and $c_2 = 0.4767k_L\mu_{D,eff}/(2\alpha k\ 300\,K)^{1/2}$ with $k_L = 2\pi q(\alpha/\mu)^{1/2}$ to be used in the equation

$$k_{cap}(T) \approx c_1 + c_2\left(\frac{T}{300\,K}\right)^{-1/2} \tag{4.1}$$

(An upper limit of k_{cap} would be provided by $14.77k_L$, see Eq. (2.10)). For all cases, Eq. (4.1) should apply well down to temperatures of the order of 10 K. The values for the parameters c_1 and c_2 given in Table 5 are determined using the present calculations for capture-controlled reaction and not relying on the experimental data. The differences to the experimental data are easily realized when the column k/k_L of Table 5 is compared with the present predicted value of 3.35 from Eq. (2.7a) with $\mu_{D,eff}/\mu_D = 1.07$, or when the sum of the columns c_1 and c_2 is compared with the column k.

We do not further discuss reactions with $k < k_{cap}(T)$ in Table 5 for which the dynamics inside the collision-complex needs to be considered (or experimental errors have to be traced). We mention that reactions of D_2O with a series of ions (as well as more reactions of H_2O) are included in Anicich's compilation [22]. These data could be analyzed in the same way as the reactions shown in Table 5.

5. Conclusions

The present work has analyzed the capture of asymmetric top dipolar rotors by arbitrary ions in various ways. First, it has provided rate constants for rotationally state-selected molecules (up to $j = 2$) in the perturbed-rotor low temperature limit (above about 0.1 K and not for ultralow temperatures in the mK range, see ref. [7]). Second, for the capture of H_2O, D_2O, and HDO by arbitrary ions it has provided an approximate, analytical representation of the capture rate constants over wide temperature ranges. The water system here serves as an example for the treatment and other asymmetric top systems should be represented in an analogous way. Since capture-control provides an upper limit for rate constants of ion–molecule reactions, experimental errors are probable when the experimental results exceed the calculated the capture rate constants. The comparison of a large group of rate constants for reactions of H_2O with ions, such as listed in the UMIST 2006 data base, revealed that about one half of these reactions appears to be capture-controlled. The temperature dependence of k_{cap} can be represented in the form $c_1 + c_2(T/300\,K)^{-1/2}$ over wide temperature ranges down to about 10 K, and the parameters c_1 and c_2 can be predicted approximately by the relationships

$$c_1 \approx 0.62k_L = 0.62 \times 2\pi q\left(\frac{\alpha}{\mu}\right)^{1/2} \tag{5.1}$$

and

$$c_2 \approx \frac{0.4767 \times 2\pi q\mu D}{(2\mu k\,300\,K)^{1/2}} \tag{5.2}$$

The replacement of μ_D by the more appropriate $\mu_{D,eff}$ requires fairly involved calculations such as performed in the present work which, however, needs to be done only once for each asymmetric top. For H_2O one has $\mu_{D,eff} \approx 1.07\,\mu_D$, for D_2O one has $\mu_{D,eff} \approx 1.06\,\mu_D$, and for HDO one has $\mu_{D,eff} \approx 1.06\,\mu_D$. The differences are within the uncertainty of the fits and calculations. If the calculations of $\mu_{D,eff}$ were not made, the assumption $\mu_{D,eff} \approx \mu_D$ would have presented a good starting point for the prediction of capture rates.

Finally we emphasize that the approach outlined in the present work for capture of asymmetric top molecules, of course, also applies to the simpler cases of capture of symmetric top and linear dipole molecules. In that case, the required numerical calculations for fixing $\mu_{D,eff}$ can resort to the analytical (approximate) adiabatic eigenvalue representations of ref. [3].

Acknowledgments

The authors thank Zdenek Herman for many years of stimulating scientific exchange and personal friendship. Financial support of this work by the EU Human Potential Program MCRTN 51230 "The Molecular Universe" is also acknowledged.

Appendix A

A.1. Molecular parameters used in the calculations

Values for H_2O, D_2O, and HDO, respectively:

$A/hc\,cm^{-1} = 27.30$, 15.17, and 23.07; $B/hc\,cm^{-1} = 14.65$, 7.327, and 9.151;
$C/hc\,cm^{-1} = 9.536$, 4.940, and 6.552; $\gamma = 0.3493$, 0.3257, 0.2840;
$\alpha/10^{-24}\,cm^3 = 1.45$, 1.45, and 1.45; $\mu_{D,b}/D = 1.857$, 1.857, and 1.730;
$\mu_{D,a}/D = 0$, 0, and 0.675.

A.2. Perturbed-rotor second-order expansion coefficients

The adiabatic channel eigenvalues $V^{cd,2}_{j,\tau,m}(R)$ for asymmetric tops interacting with ions can be obtained by matrix diagonalization. In perturbed-rotor second-order expansion they can be expressed by Eq. (3.2) with the coefficients $A_{bj\tau}(\kappa,\eta)$ and $B_{bj\tau}(\kappa,\eta)$ in analytical form given by

$$\begin{aligned}
&A_{b00} = -\frac{1}{6};\\
&A_{b1\pm1} = -\frac{1}{10(2\pm\eta)}, \qquad B_{b1\pm1} = \frac{1}{40(2\pm\eta)} \pm \frac{1}{8\eta};\\
&A_{b10} = \frac{1}{6} - \frac{4(1+\eta\kappa)}{15(4-3\eta^2+4\eta\kappa)}, \qquad B_{b10} = -\frac{1}{6} + \frac{1+\eta\kappa}{15(4-3\eta^2+4\eta\kappa)};\\
&A_{b2\pm2} = \mp\frac{\kappa \mp \sqrt{3+\kappa^2}}{15\sqrt{3+\kappa^2}\{2+\eta(\kappa\pm\sqrt{3+\kappa^2})\}} \pm \frac{6\kappa \mp 21\sqrt{3+\kappa^2} + 2\eta\{33+7\kappa^2 \mp 2\kappa\sqrt{3+\kappa^2}\}}{210\sqrt{3+\kappa^2}(3-4\eta^2 \mp 2\eta\sqrt{3+\kappa^2})},\\
&B_{b2\pm2} = \mp\frac{\kappa \pm \sqrt{3+\kappa^2}}{36\eta\sqrt{3+\kappa^2}(\kappa \mp \sqrt{3+\kappa^2})} \pm \frac{\kappa \mp \sqrt{3+\kappa^2}}{60\sqrt{3+\kappa^2}\{2+\eta(\kappa\pm\sqrt{3+\kappa^2})\}} \mp \frac{6\kappa \mp 21\sqrt{3+\kappa^2} + 2\eta\{33+7\kappa^2 \mp 2\kappa\sqrt{3+\kappa^2}\}}{1890\sqrt{3+\kappa^2}(3-4\eta^2 \mp 2\eta\sqrt{3+\kappa^2})};\\
&A_{b20} = -\frac{1}{42}, \qquad B_{b20} = \frac{1}{378} - \frac{\kappa}{27\eta};\\
&A_{b2\pm1} = \frac{1}{10(2\pm\eta)} - \frac{2\{6\mp\eta(3\mp8\kappa)\}}{105\{3+4\eta\kappa-2\eta^2(1\mp k)\}},\\
&B_{b2\pm1} = \pm\frac{1}{216\eta} - \frac{1}{40(2\pm\eta)} + \frac{2\{6\mp\eta(3\mp8\kappa)\}}{945\{3+4\eta\kappa-2\eta^2(1\mp k)\}}
\end{aligned} \tag{A.1}$$

The corresponding coefficients $A_{aj\tau}(\kappa,\eta)$ and $B_{aj\tau}(\kappa,\eta)$ can be covered by the substitutions

$$\begin{array}{ll} B \to A; & g = b \to g = a \\ j, \tau = 1, -1 \to j, \tau = 1, 0 & j, \tau = 2, 1 \to j, \tau = 2, 0 \\ j, \tau = 1, 0 \to j, \tau = 1, -1 & j, \tau = 2, 0 \to j, \tau = 2, 1 \\ \kappa \to \dfrac{3-\kappa}{1+\kappa} & \eta \to \dfrac{\eta(1+\kappa)}{2-\eta(1-\kappa)} \end{array} \tag{A.2}$$

For planar asymmetric tops, the two parameters κ and η can be expressed through a single parameter $\gamma = C/A$ (where $1/C = 1/A + 1/B$) such that $A_{bj\tau}(\kappa,\eta)$ and $B_{bj\tau}(\kappa,\eta)$ with

$$\kappa = \frac{\gamma^2 + 2\gamma - 1}{(1-\gamma)^2} \quad \text{and} \quad \eta = \frac{1-\gamma}{1+\gamma} \tag{A.3}$$

become new functions $\tilde{A}_{bj\tau}(\gamma)$ and $\tilde{B}_{aj\tau}(\gamma)$. Similarly, the substitution

$$\kappa = \frac{2 - 4\gamma + \gamma^2}{\gamma^2} \quad \text{and} \quad \eta = \frac{\gamma}{1-2\gamma} \tag{A.4}$$

into $A_{aj\tau}(\kappa,\eta)$ and $B_{aj\tau}(\kappa,\eta)$ leads to the new functions $\tilde{A}_{aj\tau}(\gamma)$ and $\tilde{B}_{aj\tau}(\gamma)$ to be used in Eq. (3.2).

References

[1] J. Woodall, M. Agúndez, A.J. Markwick-Kemper, T.J. Miller, Astron. Astrophys. 466 (2007) 1197.
[2] D.C. Clary, Ann. Rev. Phys. Chem. 41 (1990) 61.
[3] J. Troe, J. Chem. Phys. 105 (1996) 6249.
[4] M. Ramillon, R. McCarroll, J. Chem. Phys. 101 (1994) 8697.
[5] M.L. Dubernet, R. McCarroll, Z. Phys. D: At. Mol. Clust. 15 (1990) 333.
[6] T. Stoecklin, D.C. Clary, A. Palma, J. Chem. Soc. 88 (1992) 901.
[7] E.I. Dashevskaya, I. Litvin, A.I. Maergoiz, E.E. Nikitin, J. Troe, J. Chem. Phys. 118 (2003) 7313.
[8] J. Troe, J. Chem. Phys. 87 (1987) 2773.
[9] A.I. Maergoiz, E.E. Nikitin, J. Troe, V.G. Ushakov, J. Chem. Phys. 105 (1996) 6263.
[10] A.I. Maergoiz, E.E. Nikitin, J. Troe, V.G. Ushakov, J. Chem. Phys. 105 (1996) 6270.
[11] J.E. Wollrab, Rotational Spectra and Molecular Structure, Academic Press, New York, 1967.
[12] S. Golden, E.B. Wilson, J. Chem. Phys. 16 (1948) 669.
[13] R.N. Zare, Angular Momentum, Wiley Publ., New York, 1988.
[14] The misprinted factor 2 in Eq. (6.3) of ref. 8 should be replaced by 4.
[15] A.I. Maergoiz, J. Troe, Ch. Weiss, J. Chem. Phys. 101 (1994) 1885.
[16] T. Su, W.J. Chesnavich, J. Chem. Phys. 76 (1982) 5183.
[17] T. Su, J. Chem. Phys. 88 (1988) 4102;
T. Su, J. Chem. Phys. 89 (1988) 5355.
[18] J.B. Marquette, B.R. Rowe, G. Dupeyrat, G. Poissant, C. Rebrion, Chem. Phys. Lett. 122 (1985) 431.
[19] D. Smith, N.G. Adams, T.M. Miller, J. Chem. Phys. 69 (1978) 308.
[20] B.R. Rowe, J.B. Marquette, G. Dupeyrat, E.E. Ferguson, Chem. Phys. Lett. 113 (1985) 403.
[21] D.C. Clary, J. Chem. Soc. Faraday Trans. II 83 (1987) 139.
[22] V.B. Anicich, JPL Publication 03-19 (2004).